 doi:10.20944/preprints202011.0440.v1

Article

Methotrexate gold nanocarriers: Loading and release study. Its activity in colon and lung cancer cells

B. Álvarez-González[1], M. Rozalen[1*], M. Fernández-Perales[1], M.A. Álvarez[2] and M. Sánchez-Polo[1]

[1] Department of Inorganic Chemistry, Faculty of Science, University of Granada, Campus Fuentenueva s/n 18071 Granada, Spain; abeatriz@ugr.es (B.A.-G); marisarozalen@ugr.es (M.R.); mariafeper@ugr.es (M.F.-P); mansanch@ugr.es (M.S.-P)

[2] Department of Inorganic and Organic Chemistry, Faculty of Science University of Jaén, Campus las Lagunillas s/n, 23071, Jaén, Spain; malvarez@ujaen.es (M.A.Á)

* Correspondence: marisarozalen@ugr.es (M.R.); Tel.: +34-958-248526

Abstract: In the present study the synthesis of gold nanoparticles (AuNPs) loaded with methotrexate (MTX) has been carried out in order to obtain controlled size and monodispersed nanocarriers, around 20nm. Characterization study shows metallic AuNPs with MTX polydispersed on the surface. MTX is linked by a replacement of citrate by the MTX carboxyl group. The drug release profiles showed faster MTX release when it is conjugated, which leads to the best control of plasma concentration. Also, the enhanced release observed at pH 5 could take advantage of the pH gradients that exist in tumor microenvironments to achieve high local drug concentrations. AuNPs-MTX conjugates were tested by flow cytometry against lung (A-549) and colon (HTC-116) cancer cell lines. Results for A-549 showed a lighter dose-response effect than for colon cancer ones. This could be related to the presence of folate receptors in line HTC-116 on the contrary than line A-549, supporting the specific uptake of folate-conjugated AuNPs-MTX by folate receptor positive tumor cells. Conjugates exhibited considerably higher cytotoxic effects compared with the effects of equal doses of free MTX. Anexin V-PI test sustain as cell death mechanism apoptosis, which is normally disabled in cancer cells.

Keywords: Au nanoparticles, nanocarriers, methotrexate, anticancer drug, chemotherapeutics, controlled release.

1. Introduction

Gold nanoparticles (AuNPs) have been investigated and established for its use as anti-neoplastic, anti-arthritic, antibacterial and antidiabetic agent. Moreover, AuNPs are an excellent delivery vehicle for different therapeutic agents, mainly anticancer drugs such as cisplatin, doxorubicin, tamoxifen, paclitaxel or methotrexate.

Their unique shape (spherical, rod shape, core shell, nanorods…) with varied sized from 1 to 100nm, surface properties, inert nature, high biocompatibility and non-cytotoxicity represent important advantages. Furthermore, large functional surface to mass ratio increases efficient drug payload avoiding the cytotoxic effects in healthy tissues caused by overdoses [1] The drug attachment can be accomplished by covalent binding, encapsulation, electrostatic absorption and other non-covalent assemblies [2].

MTX is an analogue of folic acid, which main difference is that folic acid has a hydroxyl group at the 4-position of the pyridine ring while MTX present an amine group at the same position. Due to the structural similarity cells internalize MTX through similar transport systems as folates, inhibiting dihydrofolate reductase (DHFR), a critical enzyme in the folic acid cycle and key to

 doi:10.20944/preprints202011.0440.v1

regulating homeostasis, leading to reduced cell viability and cell death. As folate receptors are overexpressed on the cell membranes of many types of cancer cells, MTX has proven to be an effective targeting agent [3,4] and showed a potent anticancer effect. It has been used for the treatment of acute leukemia, osteogenic sarcoma, choriocarcinoma, breast cancer, pulmonary and epidermoid carcinoma and intratracheal chemotherapy. It is also used in bone marrow transplantation, sever psoriasis and rheumatoid arthritis [5]. However, its clinical application is limited due to its poor solubility, short half-life bloodstream and rapid diffusion throughout the body [6].

The existing studies [7-12] have shown that linking MTX to AuNPs allows for efficient and selective uptake, a property unique to nanocarriers, enhancing therapeutic efficacy and lowering effective doses. For instance, free MTX effect on lung cancer cells is seven times less than Au-MTX conjugated nanoparticles synthetized by Cheng et al. [8].

Controlled drug release can be achieved by: i) passive targeting through accumulation based on enhanced permeability and retention effect (EPR) observed for relatively large sized nanoparticles (~15-100 nm) [13-17] in solid tumor models or ii) active targeting using various payload release mechanism including pH change [18,19] or triggering by endogenous glutathione utilizing thiol-to-thiol ligand exchange [20-22]. Because ligand exchange is based upon competitive affinity to gold surface between original and incoming ligands [21] MTX can be used not only as a drug but also as a potential targeting ligand [10] because can be directly bound to AuNPs via carboxylic group to form conjugates MTX-AuNPs. In vitro cytotoxicity in lung tumor cells showed a higher accumulation of MTX conjugated with AuNPs compared with equal doses of free MTX. Moreover MTX-AuNPs suppressed the tumor growth in a mouse ascites model of Lewis lung carcinoma.

Tran et al. [11] synthetized AuNPs using MTX as both reducing agent and capping molecule obtaining various sizes between 3-20 nm. To examine anticancer effects, they applied the lactate dehydrogenase (LDH) and MTT assays demonstrating that small size (3 nm) MTX-AuNPs exhibited considerably high cytotoxic effect in human choriocarcinoma cell lines compared to the effects of equal doses of free MTX

Murawala et al. [10] investigated the efficiency of MTX loaded BSA capped AuNPs (Au-BSA-MTX) in preventing the propagation of breast cancer cell lines (MCF-7) based on MTT and Ki-67 proliferation assays.

Bessar et al. [7] designed water soluble gold nanoparticles functionalized by sodium 3-mercapto-1-propansulfonate (Au-3MPS) and loaded with MTX, in order to improve solubility, stability and biodistribution of the drug for psoriasis treatment. They showed a fast release (80 % in an hour) and were tested successfully on C57BL/6 mouse normal skin to trace the absorption behavior.

Wang et al. [12] synthetized Au-MTX conjugates using a hydrothermal growth method to lead into nanochains and discrete nanoparticles around 30 nm. Compared with nanochains the discrete nanoparticles showed almost equal drug loading capacity (between 8.6-25.1 %) but higher control of drug release, colloidal stability and in vitro anticancer activity (A-549 cell line/lung cancer).

In spite of the progress, AuNPs synthesis still present some drawbacks as monodispersity, unsuccessful functionalization and stability, lack of size homogeneity, limited opsonization or plasma and blood internalization.

With this background, the main objective of the present study is to synthesize and characterize discrete, controlled size methotrexate gold nanoparticles (AuNPs-MTX), using as reduction agent citrate, to be used as nanocarriers of MTX. By one hand the anticancer activity has been tested by studying in vitro cytotoxicity of lung (A-549) and colon cancer (HTC-116) cell lines. By the other hand we have proposed an AuNPs-MTX formation mechanism and fitted the drug release dataset to a pharmacokinetic model to how to maintain MTX concentration in blood or in target tissues.

 doi:10.20944/preprints202011.0440.v1

2. Results and Discussion

2.1. Characterization of AuNPs and AuNPs-MTX

2.1.1. UV-Vis spectroscopy

The optical properties of the as-prepared AuNPs and AuNPs-MTX conjugates measured by UV-Vis adsorption are depicted in Figure 1. Free MTX exhibit three characteristics.

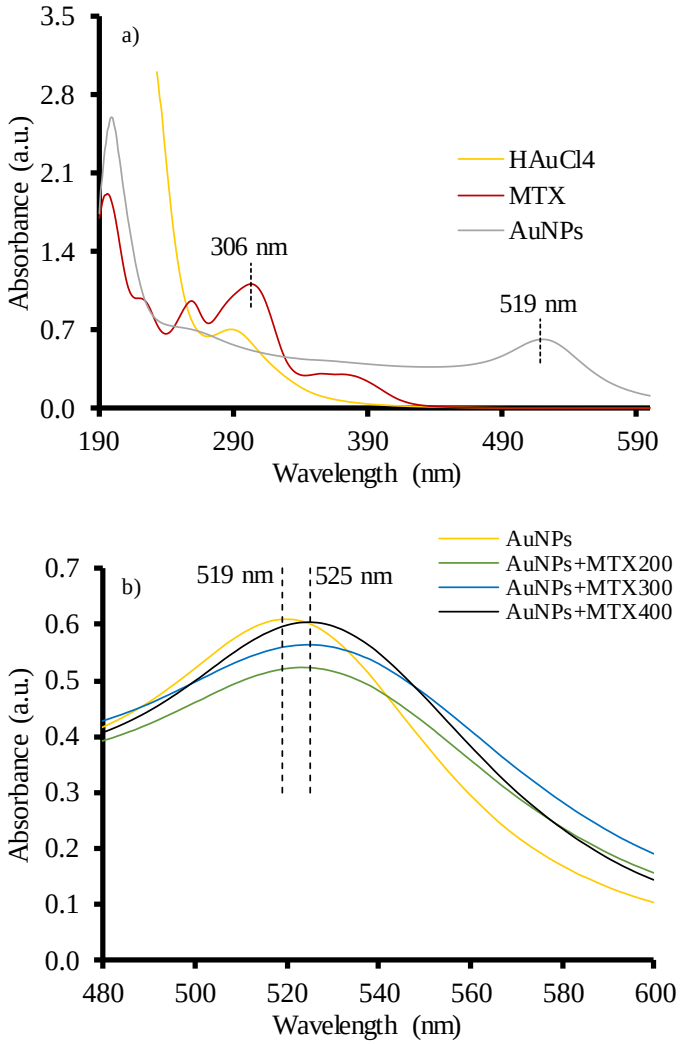

Figure 1. a) Comparative UV-Vis absorption spectra of free MTX, $HAuCl_4$ and AuNPs. b) Absorption spectra of AuNPs-MTX with different concentrations of MTX.

Absorption peaks centered at 258, 306 and 372 nm (Figure 1a). $HAuCl_4$ present a peak around 300 nm which disappeared emerging a new peak at 519 nm corresponding with the surface resonance plasmon band (SPR) of AuNPs [9,10,12,26]. Figure 1b shows a bathochromic shift around 525 nm for the AuNPs-MTX conjugates, which indicates an increase in size particle [27] and also a modification in the nanoparticles surface [28]. This could be due to the chemical absorption of MTX into the AuNPs surface, justifying the band shift from 519 to 525 nm [8-10,12].

2.1.2. X-Ray Diffraction and FTIR analysis

AuNPs and AuNPs-MTX revealed the same typical XRD pattern (Figure 2a) characterized by five diffraction peaks located at 38.16º (1 1 1), 44.36º (2 0 0), 64.74º (3 1 1), 77.6º (3 1 1) and 81.92º (2 2 2) confirming a gold crystalline phase with face centered cubic (FFC) geometry (JCPDS 04-0784).

The FTIR spectra of free MTX, AuNPs and AuNPs-MTX400 are shown in Figure 2b, confirming the formation of MTX conjugate. The peak at 3407 cm^{-1} for free MTX indicates the presence of an –

 doi:10.20944/preprints202011.0440.v1

NH group. Absorptions at 2997 and 2921 cm^{-1} correspond with the existence of carboxylic. Peaks in the region of 1675-1500 cm^{-1} can be attributed to vibration of C=C in the aromatic ring and R-NH_2 vibrations, while peaks at 1480 and 1200 cm^{-1} represent the stretching vibration of the C-C or C-H bonds [29]. Compared with free MTX, the FTIR spectrum of AuNPs-MTX exhibits similar peaks as a consequence of the interaction between AuNPs and MTX, indicating the successful uploading of MTX into the gold nanoparticles, as observed previously in literature [7,11].

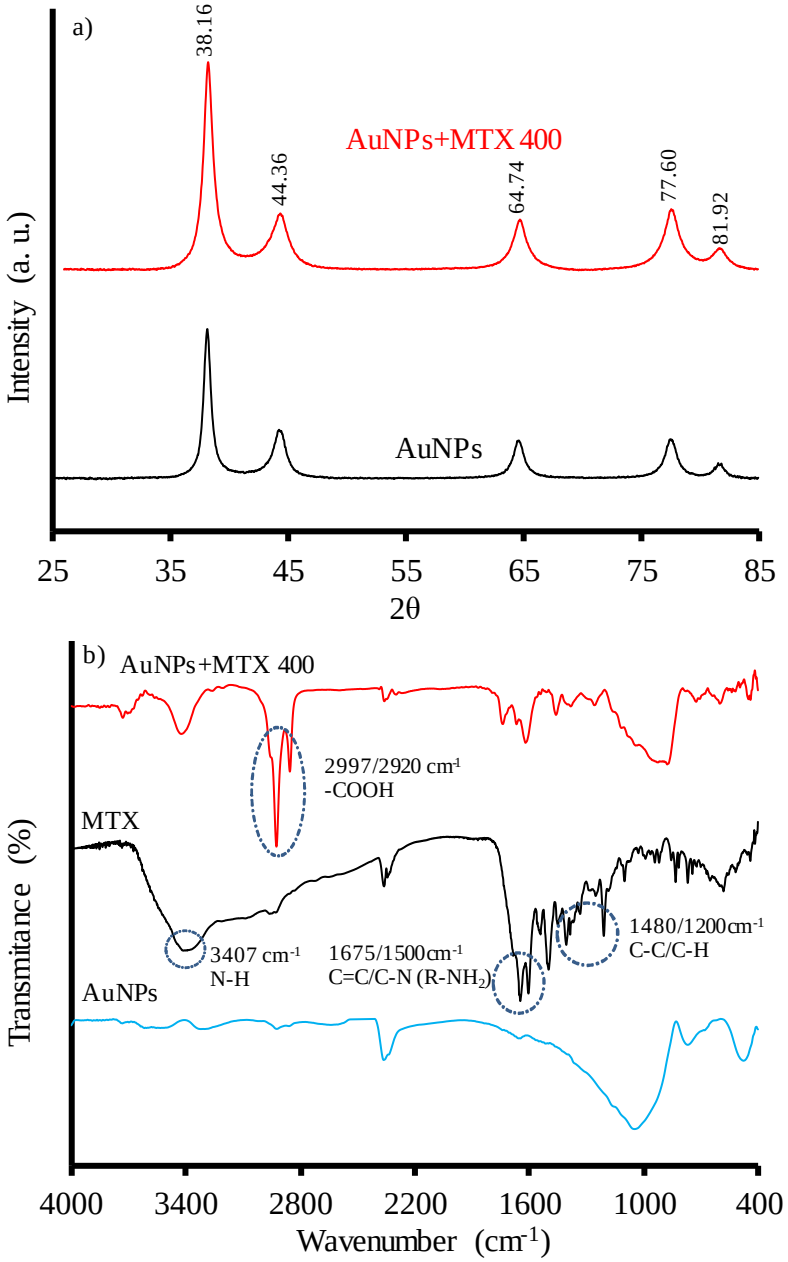

Figure 2. a) XRD diffractograms of AuNPs and AuNPs-MTX400. b) FTIR spectra of free MTX, gold nanoparticles (AuNPs) and MTX-conjugates (AuNPs-MTX400).

2.1.3. HRTEM Microscopy

The morphology of synthesized AuNPs and AuNPs-MTX was examined by HRTEM analysis. Images in Figure 3 (A-C) confirmed the formation of homogeneous size, mostly spherical, and highly dispersed gold nanoparticles.

Preprints (www.preprints.org) | NOT PEER-REVIEWED | Posted: 16 November 2020 doi:10.20944/preprints202011.0440.v1

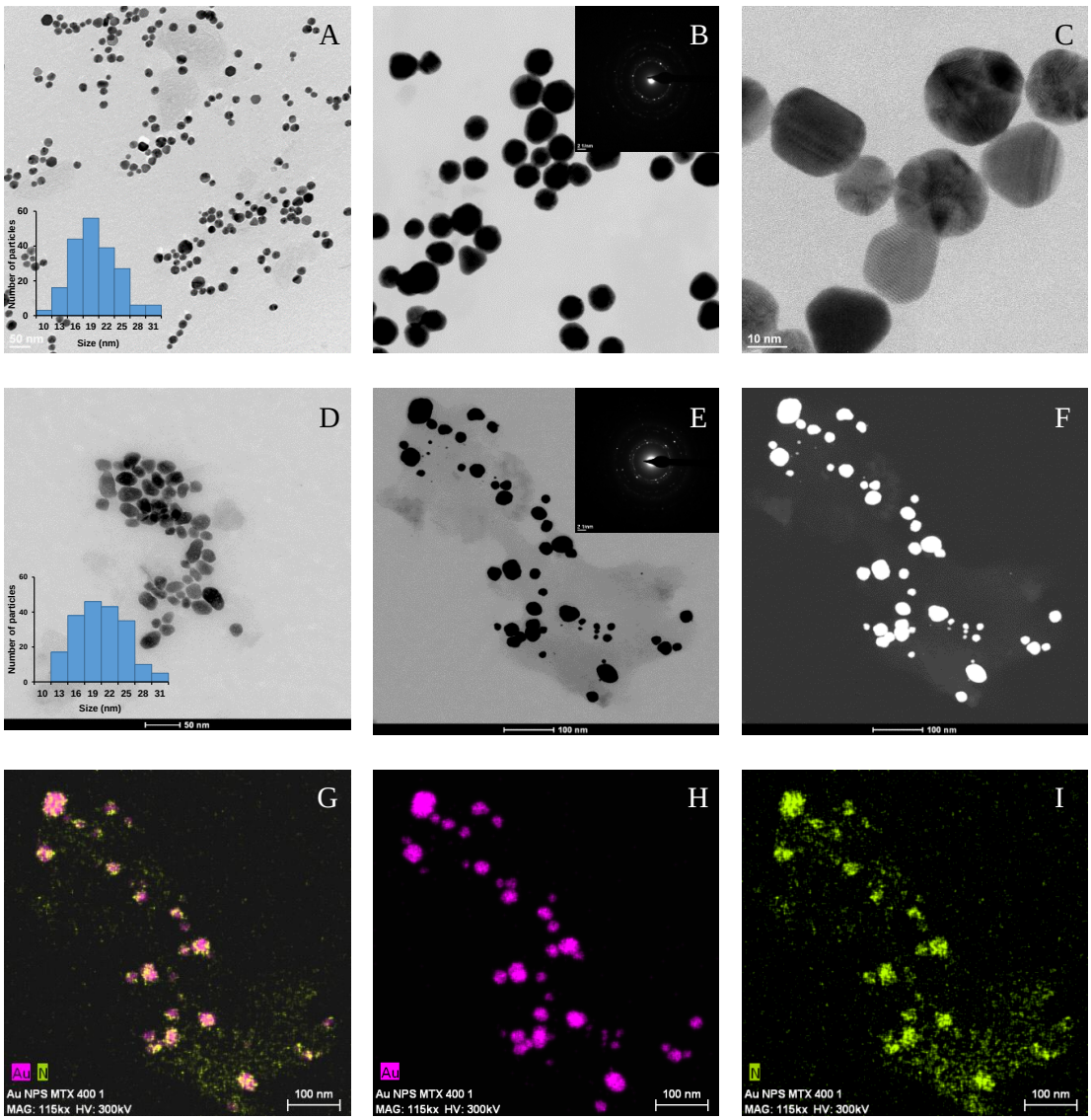

Figure 3. (A) HAADF image of a representative group of AuNPs. (B) SAED image showing the presence of a gold nanocrystalline phase (C) HRTEM lattice fringe image of AuNPs showing multiple domains. (D) HAADF image of a representative group of AuNPs-MTX. (E) SAED image showing the presence of a gold nanocrystalline phase Maps for relative distribution of the elements (pink = Au and green = N) jointly shown.

The calculated average size was 18.40 ± 4.75 with a narrow distribution range between 7-19 nm, as shown in histogram (Figure 3A). SAED image (Figure 3B) confirmed the presence of a crystalline gold phase, with distances of 2.35 and 2.09 Å corresponding with (1 1 1) and (2 0 0) planes, which is in accordance with XRD results. Finally, high resolution images (Figure 3C) showed a polycrystalline domains for spherical particles [30].

The addition of MTX does not lead to significant changes regarding to morphology or size, as just a SPR slight shift from 520 to 525 nm is observed. A representative sample of AuNPs-MTX400 confirms the formation of spherical monodisperse nanoparticles with a similar average size of 19.32 ± 4.96 nm and distribution range between 10-31nm (Figure 3D). The crystalline nature is also observed in SAED image (Figure 3E), where a group of gold nanoparticles appeared covered with MTX. This is confirmed with the chemical element mapping analysis (Figure 3G-I) pointing out a homogeneous distribution of Au and N (as an indicator of the presence of MTX) in the sample. N was not distributed in layers but along the sample which suggested the formation of AuNPs-MTX

Preprints (www.preprints.org) | NOT PEER-REVIEWED | Posted: 16 November 2020 doi:10.20944/preprints202011.0440.v1

conjugates. EDX analysis (Figure 4b) also confirmed the presence of gold and nitrogen, as an indicator of the presence of MTX.

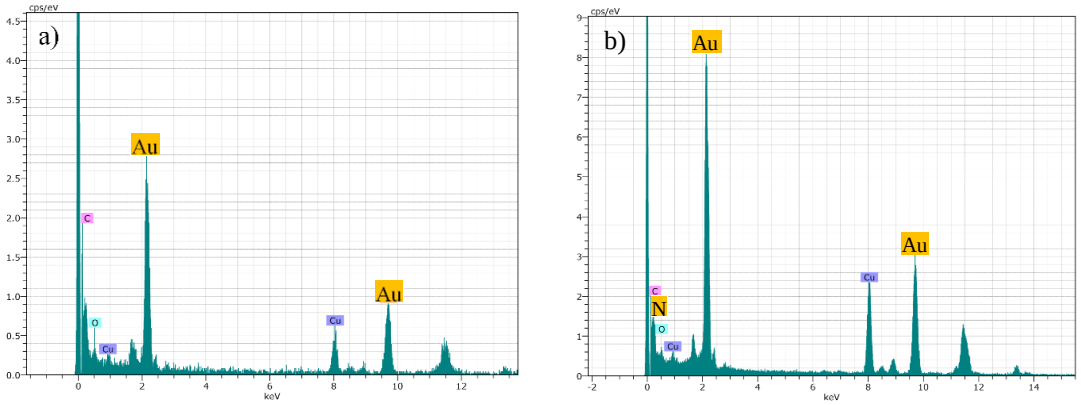

Figure 4. a) EDX analysis of AuNPs confirm the presence of gold. b) EDX analysis for AuNPs-MTX400 confirmed the presence of N as indicator of MTX presence.

2.1.4. X-Ray Photoelectron Spectroscopy (XPS)

Chemisorption of MTX on the surface of AuNPs was explored thought XPS spectra of MTX in a pure solid form as well as in the adsorbed condition (AuNPs-MTX400). Figure 5 showed the high resolution XP spectra in the C 1s, O 1s N 1s and Au 4f for free MTX, AuNPs and AuNPs-MTX400.

For free MTX, in the region C 1s region (Figure 5a) four peaks were identified at: i) 284 eV corresponding with sp^2 hybridized carbon (C=C) ii) 285.4 eV corresponding with sp^3 hybridized carbon (C-C) and C-N bonds, iii) 288.4 eV assigned to C-O bonds from hydroxyl/ether groups, iv) 288.4 eV assigned to carboxyl (-COOH) moiety. Concerning the O 1s region (Figure 5 d) two peaks are identified around 530.5 and 532 eV corresponding with the oxygen atoms in the ring carbonyl (>C=O) and the carboxyl (-COOH) moieties, respectively [31,32] whereas the N 1s region, just a peak at 398.7 eV was identified (Figure 5g) whereas for. Otherwise, XPS spectra in Au 4f regions showed two peaks with a bond energy of 83.5 and 87.2 eV assigned to Au $4f_{7/2}$ and Au $4f_{5/2}$ respectively (Figure 5c).

After the adsorption of MTX in the AuNPs surface, the C 1s peak located at 288.2 eV and derived from the carboxylic carbon is shifted until 288.7 eV and can be attributed to the carboxylate group, -COO-, (Figure 5b). This is in accordance with the results obtained by [8] providing evidence that MTX is adsorbed chemically on the AuNPs surface as a carboxylate form. Moreover, oxygen peak on the carboxylate group results in the shift to lower bonging energies, as a consequence of the increase of electron density of oxygen on the carboxylate group respect to the carboxylic group (Figure 5e). Au 4f and N 1s regions remained unchanged (Figures 5f and 5h). Based on XPS results and the hypothesis of Chen et al. [8] where MTX exchanges the citrate molecules on the AuNPs surface and bonding to AuNPs surface through a covalent bond.

Covalent bonding of therapeutic agents on nanocarriers is usually favored because the bond strength makes the NPs drug conjugates highly stable and therefore is most likely to be disrupted only under harsh environments inside lysosomes [33]. MTX-conjugated NPs were believed to be taken up into cells to a more degree by the human folate receptor than free MTX [8].

Preprints (www.preprints.org) | NOT PEER-REVIEWED | Posted: 16 November 2020 doi:10.20944/preprints202011.0440.v1

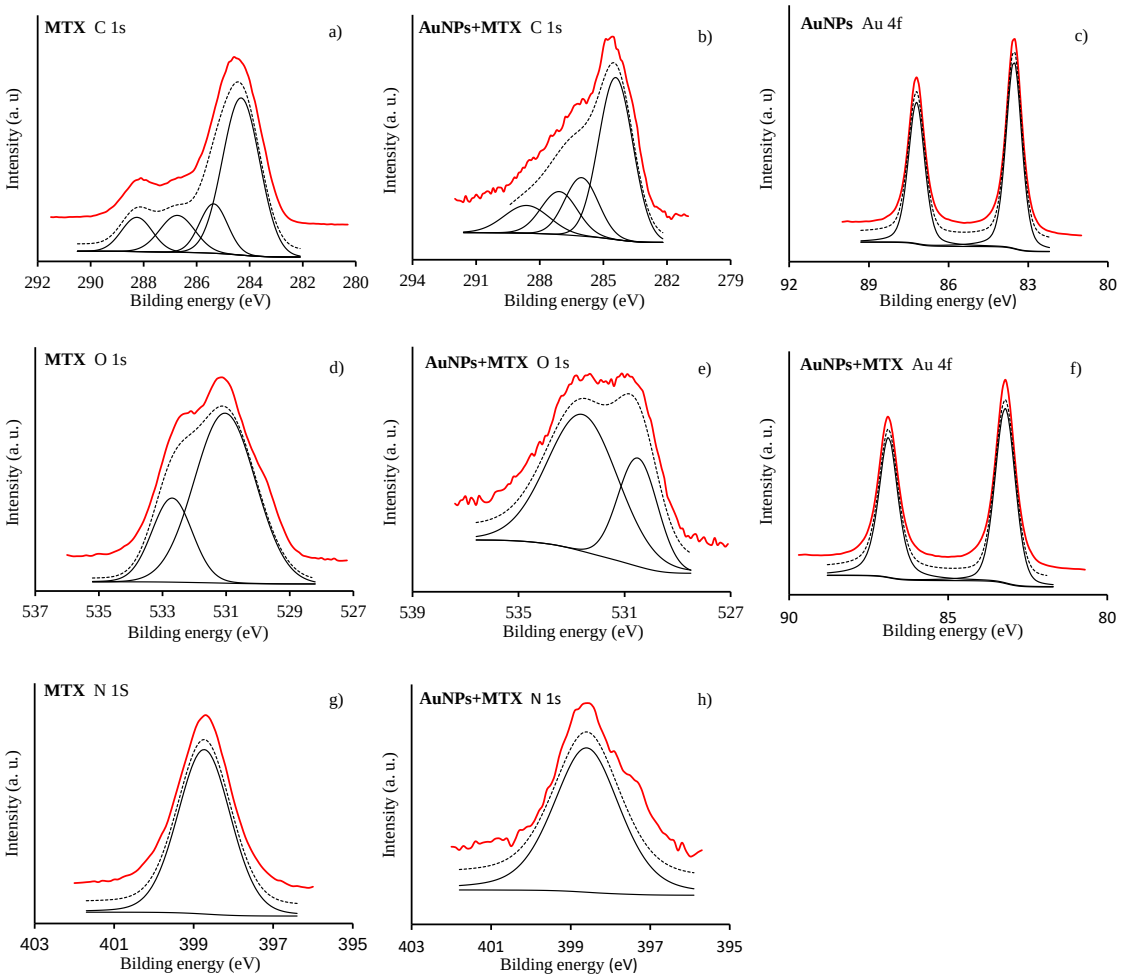

Figure 5. XPS spectra of regions C 1s, O 1s, N 1s and Au 4f of MTX, AuNPs and AuNPs-MTX400

2.2. Stability analysis of AuNPs-MTX conjugates

Synthesized gold colloids with different amounts of MTX where tested for long term colloidal stability by using UV-Vis absorption spectroscopy. Samples were storaged in the darkness at 4 ºC. As it is observed in Figure 6, AuNPs and the three AuNPs-MTX conjugates maintained the position of surface plasmon resonance (519 and 525 nm respectively) and intensity during more than a month. MTX peaks around 280 and 308 nm also remained unaltered, confirming the stability of the synthetized conjugates. This is in accordance with the results obtained in other studies [27].

Preprints (www.preprints.org) | NOT PEER-REVIEWED | Posted: 16 November 2020 doi:10.20944/preprints202011.0440.v1

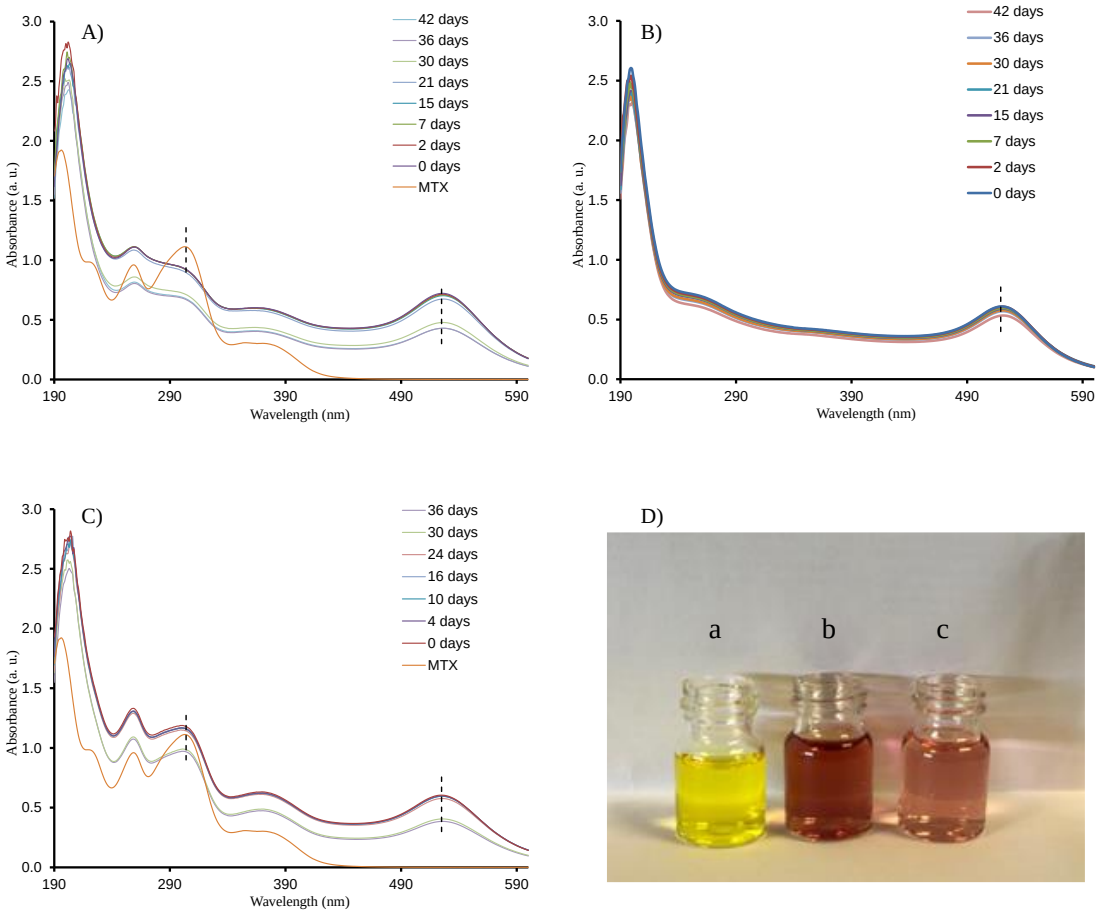

Figure 6. Colloidal stability test for: A) AuNPs-MTX400; B) AuNPs-MTX200 and C) AuNPs. D) Short term stability (24 h) in PBS with 10% FBS of AuNPs (c) and AuNps-MTX400 (b) and $HAuCl_4$ included as a reference. In all cases they are not stable when diluted by only phosphate buffered solution (PBS), while in the presence of fetal bovine serum (FBS) the particles are stable at least for 24 h.

Short term study confirmed that they were not stable when diluted by only phosphate buffered solution (PBS), while in the presence of fetal bovine serum (FBS) the particles are stable at least for 24 h without the addition of DMEM. As might be expected, this implies that AuNPs and AuNPs-MTX synthetized are sensitive to high salts contents, but FBS can stable nanoparticles and keep their dispersity.

2.3. Quantification and drug release study

The amount of MTX conjugated on the AuNPs surface is 15.1 %, 19.4 % and 23.6 % for the samples AuNPs-MTX200, AuNPs-MTX300 and AuNPs-MTX400 respectively.

In vitro release profiles of MTX from AuNPs prepared at different concentration have been investigated and shown in Figure 7. As it is observed free MTX is released until 80 % in the first 4 h reaching 100 % before 8 h (Figure 7a) but when MTX is conjugated with AuNPs release time increase until 200 h (Figure 7b). The obtained percentage of released drug increase following the sequence: AuNPs-MTX400 (78 %) > AuNPs-MTX300 (43 %) >AuNPs-MTX200 (35 %).

Results obtained in Figure 7c showed a clear pH effect with a faster release at pH 5 (95 % after 200 h) compared with the 77 % reached at pH 7.6. Consequently at the tissue level, synthetized AuNPs-MTX400 could take advantage of the pH gradients that exist in tumor microenvironments to achieve high local drug concentrations, as it has been observed in other studies [34, 35]. Finally, at the intracellular level, pH-responsive AuNPs also could escape acidic endo-lysosomal compartments

Preprints (www.preprints.org) | NOT PEER-REVIEWED | Posted: 16 November 2020 doi:10.20944/preprints202011.0440.v1

for cytoplasmic drug release [36,37] where MTX could inhibit the DHRF enzyme breaking the folic acid cycle [33].

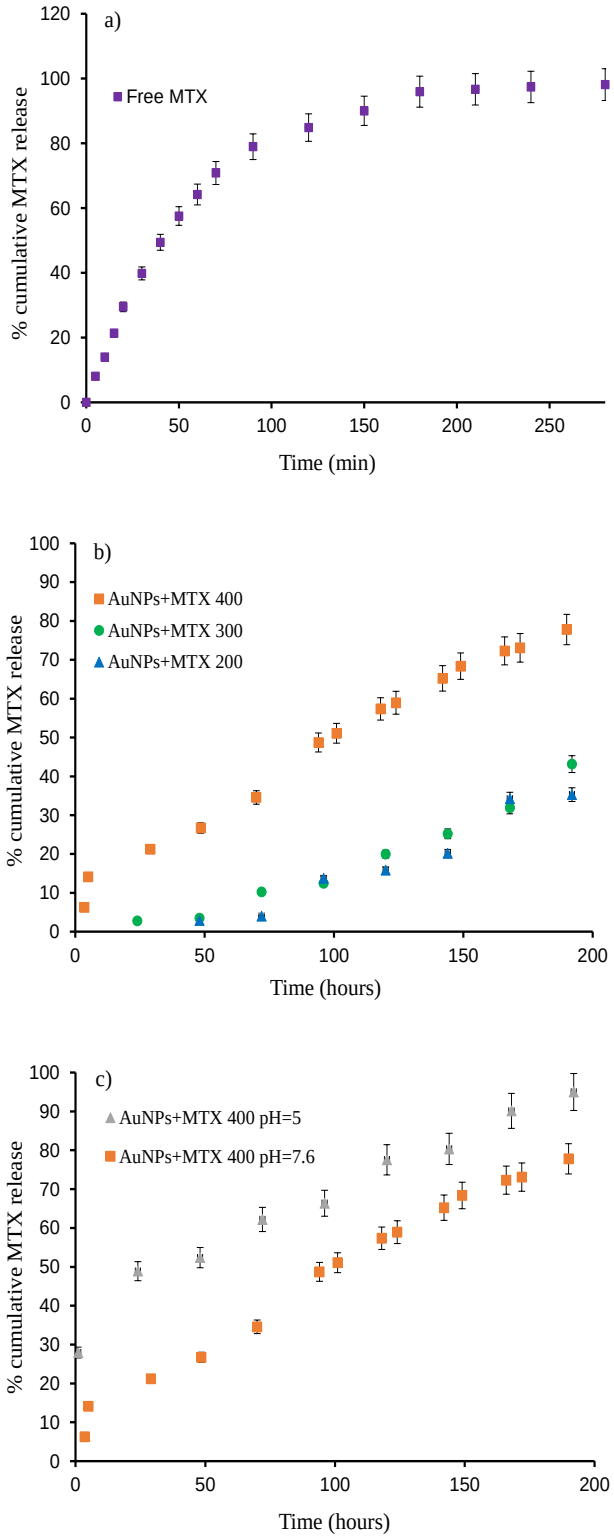

Figure 7. The release profiles of: (A) Free MTX; (B) AuNPs-MTX 400, AuNPs-MTX 300 and AuNPs-MTX 200; (C) AuNPs-MTX 400 at pH 7.6 and pH 5

2.4. Kinetic modeling

The mechanism of MTX conjugation have been tested applying different kinetic models, in order to fit the experimental cumulative drug release data (Table 1).

Preprints (www.preprints.org) | NOT PEER-REVIEWED | Posted: 16 November 2020 doi:10.20944/preprints202011.0440.v1

The release of free MTX fitted a first-order model represented by the following equation:

$$\log M = \log M_0 - k \cdot \frac{t}{2.303} \qquad (1)$$

where Mo is the initial concentration of drug, k is the first order rate constant and t is the experiment time.

MTX released from AuNPs-MTX200, Au-MTX 300 and AuNPs-MTX400 followed a zero-order model, representative from drug dissolution from dosage forms that do no disaggregate and release the drug slowly following the equation:

$$Q_t = Q_0 + K_0 \cdot t \qquad (2)$$

where Q_t is the amount of drug dissolved in time t, Q_0 is the initial amount of drug in the solution and K_0 is the zero-order release constant expressed in units of concentration/time.

Finally MTX released at acid fitted a Hixson-Crowell model, represented by the equation:

$$W_t^{1/3} = W_0^{1/3} - \kappa \cdot t \qquad (3)$$

where W_0 is the initial amount of drug in the pharmaceutical dosage form, W_t is the remaining amount of drug in the pharmaceutical dosage form at time t and κ is a constant incorporating the surface-volume ratio.

Dataset for free MTX was fitted to a first order kinetic model obtaining a value of k = 0.0026 min^{-1} with a regression coefficient of r^2 = 0.988 while AuNPs-MTX200, AuNPs-MTX300 and AuNPs-MTX400 were fitted to a zero-order kinetic model obtaining values of k = 0.0034, 0.004 y 0.006 mg/min and regression coefficients of r^2 = 0.9116, 0.9757 y 0.9801, respectively. Obtaining a zero-order release, in which a drug is released at a constant rate, is the ultimate goal of all controlled-release drug-delivery mechanisms. It leads, in principle, to the best control of plasma concentration and offers several advantages, including improved patient compliance and reduction in the frequency of drug administration [38]. Finally, acid pH release of AuNPs-MTX400 was fitted to a Hixson-Crowell model obtaining a value of κ = 0.0002 $mg^{1/3}$/min with a regression coefficient of r^2 = 0.9559.

According to the results obtained, we selected the sample AuNPs-MTX400 to carry out the *in vitro* anticancer activity tests.

Table 1. Calculated parameters and correlation coefficients (r2) of different models of release kinetics of AuNPs and the corresponding MTX conjugates synthesized in this study.

Model	**First order**		**Zero order**		**Hixson-crowell**	
	r^2	k_H (h^{-1})	r^2	k_H (h)	r^2	k_H (h)
Free MTX	**0.9885**	0.9111	0.9609	0.9009	0.946	0.013
AuNPs-MTX200	0.8857	0.0025	**0.9116**	0.0034	0.8952	0.00006
AuNPs-MTX300	0.9409	0.0035	**0.9757**	0.004	0.9553	0.00008
AuNPs-MTX400	0.8428	0.0112	**0.9801**	0.006	0.9594	0.0002
AuNPs-MTX400 pH	0.933	0.0128	0.8632	0.0066	**0.9559**	0.0002

2.5. In vitro anticancer activity

The cytotoxic effect of the free MTX, AuNPs and AuNPs-MTX400 were tested against colorectal cancer (HTC-116) and human lung carcinoma (A-549) cell lines. Dose response curve for free MTX showed IC_{50} values of 2.3, 0.37 and 0.15mM after 12, 24 and 48 hours for HTC-116 cell line (Table 2).

Preprints (www.preprints.org) | NOT PEER-REVIEWED | Posted: 16 November 2020 doi:10.20944/preprints202011.0440.v1

Results obtained for lung cancer (A-549) does not showed any effect at the concentrations studied after 12 or 24 hours, however after 48 hours the IC_{50} calculated is 0.10mM, reflecting a lower sensitivity and slower response time for this cell line.

Table 2. IC50 values of free MTX at 12, 24 and 48h for cell lines HTC-116 and A-549

[MTX] IC_{50}	HTC-116		[MTX] IC_{50}	A-549	
time	mM	µg/ml	time	mM	µg/ml
12 h	2.313	1051	12 h	-	-
24 h	0.371	169	24 h	-	-
48 h	0.153	70	48 h	0.100	45

Interestingly, results obtained for A-549 cell line showed a lighter dose-response effect (Figure 8). This could be related to the presence of folate receptors in line HTC-116 on the contrary than line A-549, supporting the specific uptake of folate-conjugated AuNPs-MTX by folate receptor positive tumor cells.

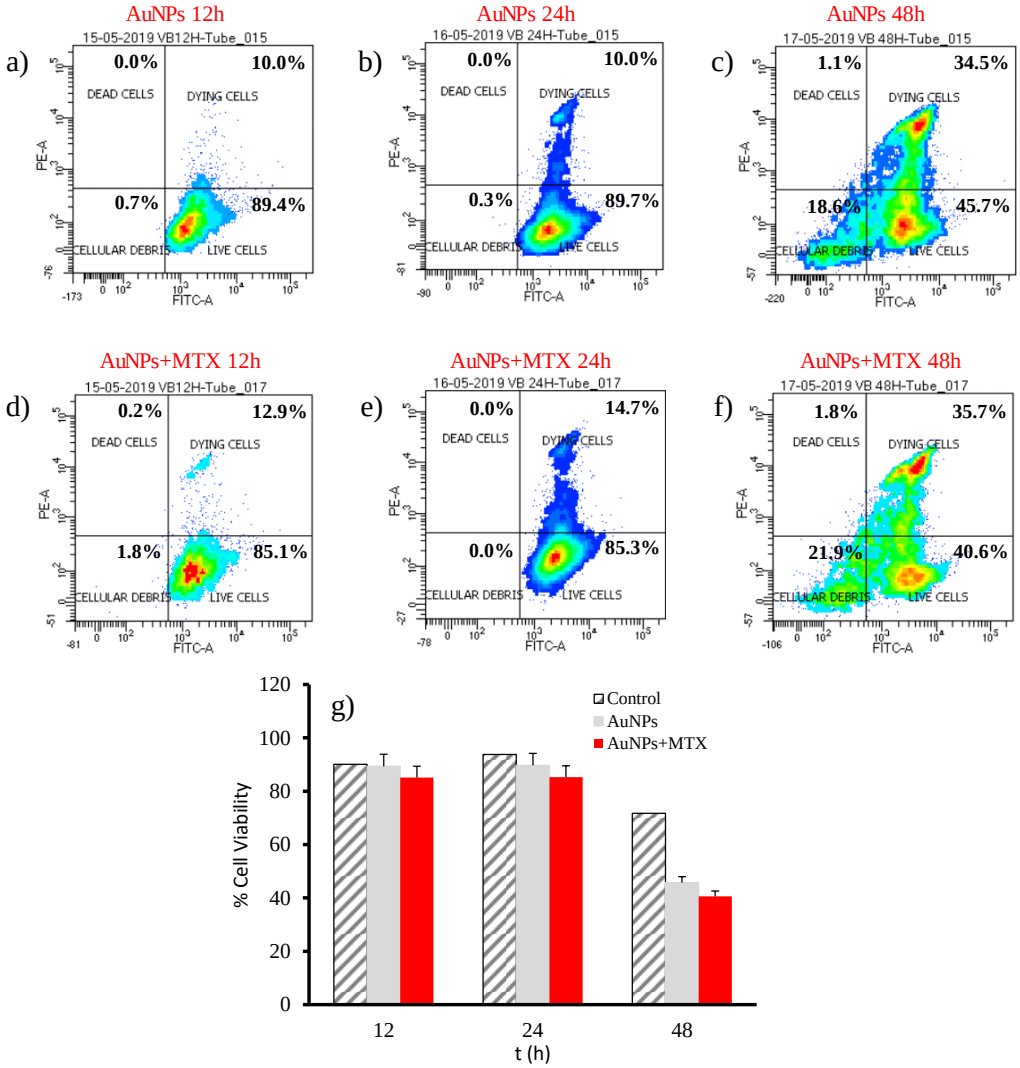

Figure 8. Percentage of cell viability obtained by flow cytometry for the A-549 cell line.

Preprints (www.preprints.org) | NOT PEER-REVIEWED | Posted: 16 November 2020 doi:10.20944/preprints202011.0440.v1

In accordance with this hypothesis, results obtained for A-549 cell line for AuNPs as well as AuNPs-MTX400 did not show a significant effect decreasing the percentage live cells at 12 or 24 exposure hours (Figure 8). After 48 hours AuNPs and AuNPs-MTX400 showed a significant cytotoxic activity decreasing the percentage of live cells until 28,5% and 25.9 % respectively.

For HTC-116 cell line AuNPs showed a significant effect decreasing the % live cells from 85.6 to 52.3 % after 12 and 48 exposure hours respectively (Figures 9a and 9c). For AuNPs-MTX400 this percentage decrease until a 40.9 % after 48 exposure hours. This is confirmed by the IC_{50} calculated (Figure 9g), which also decreased from 70 µg/mL for AuNPs to 37.5 µg/mL when MTX is conjugated with AuNPs, lowering the IC_{50} half of the free MTX and confirming the therapeutic effect of the conjugate for this cell line.

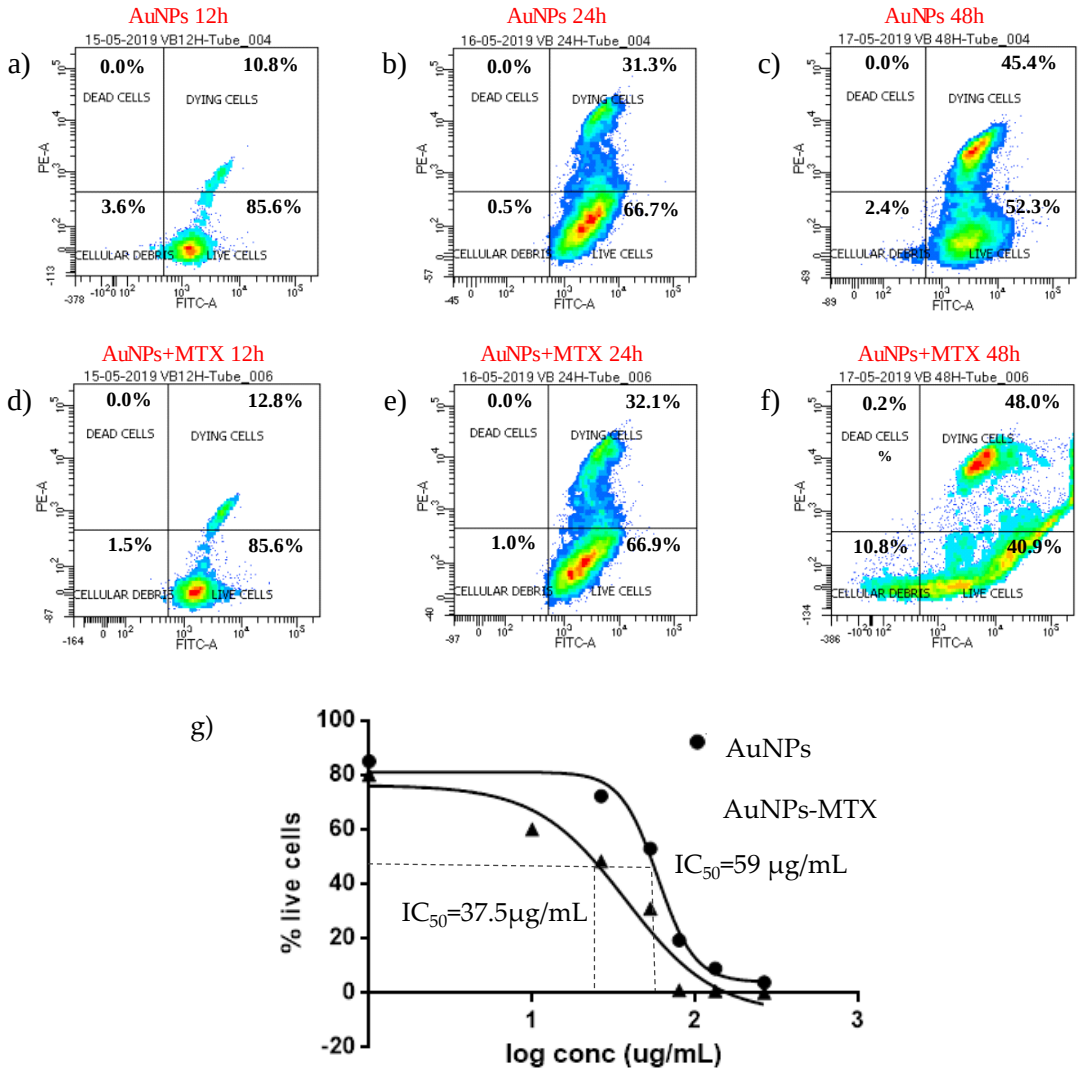

Figure 9. Percentage of cell viability for AuNPs and AuNPs-MTX400 equivalent concentrations obtained by flow cytometry for the HTC-116 cell line after 12 (a-d), 24 (b-e) and 48 (c-f) incubation hours. g) Calculated IC_{50} for equivalent concentrations of AuNPs and AuNPs-MTX400 after 48 hours of incubation.

Finally, to determine the level of apoptosis induced by AuNPs and AuNps-MTX400 was evaluated by flow cytometry density plots showing annexin V (X-axis) and propidium iodide (Y-axis) staining of HTC-116 cells (Figure 10). The right lower quadrant represents annexin V positive/propidium iodide (PI) negative staining indicating early apoptosis. The right upper

Preprints (www.preprints.org) | NOT PEER-REVIEWED | Posted: 16 November 2020 doi:10.20944/preprints202011.0440.v1

quadrant represents both high annexin V and PI staining indicating late apoptosis and the left upper quadrant represents low annexin V and high PI staining indicating necrosis. The left lower quadrant indicates viable cells. The representative density plots demonstrate dual staining after no treatment (Figure 10a) treatment with AuNPs (Figure 10b) and same concentration treatment with AuNPs-MTX400 (Figure 10c). This latter exhibited improved cytotxicity compared to the individual AuNPs at all tested concentration. Finally, the data presented in Figure 10e sustains that cell death is mostly from apoptosis to necrosis for the cell line HTC-116. As most tumour cells have presumably disabled apoptosis to achieve a malignant state, cancer cells should be more resistant to DNA-damaging anticancer agents than the normal cells from which they arose [39]. In conclusion, AuNPs-MTX tested in this study showed an improved cytotoxic effect against HTC-116 cell line compared with free MTX, inducing apoptosis as main mechanism of cell destruction, which could be a major contributor to anti-cancer therapy induced killing of tumor cells.

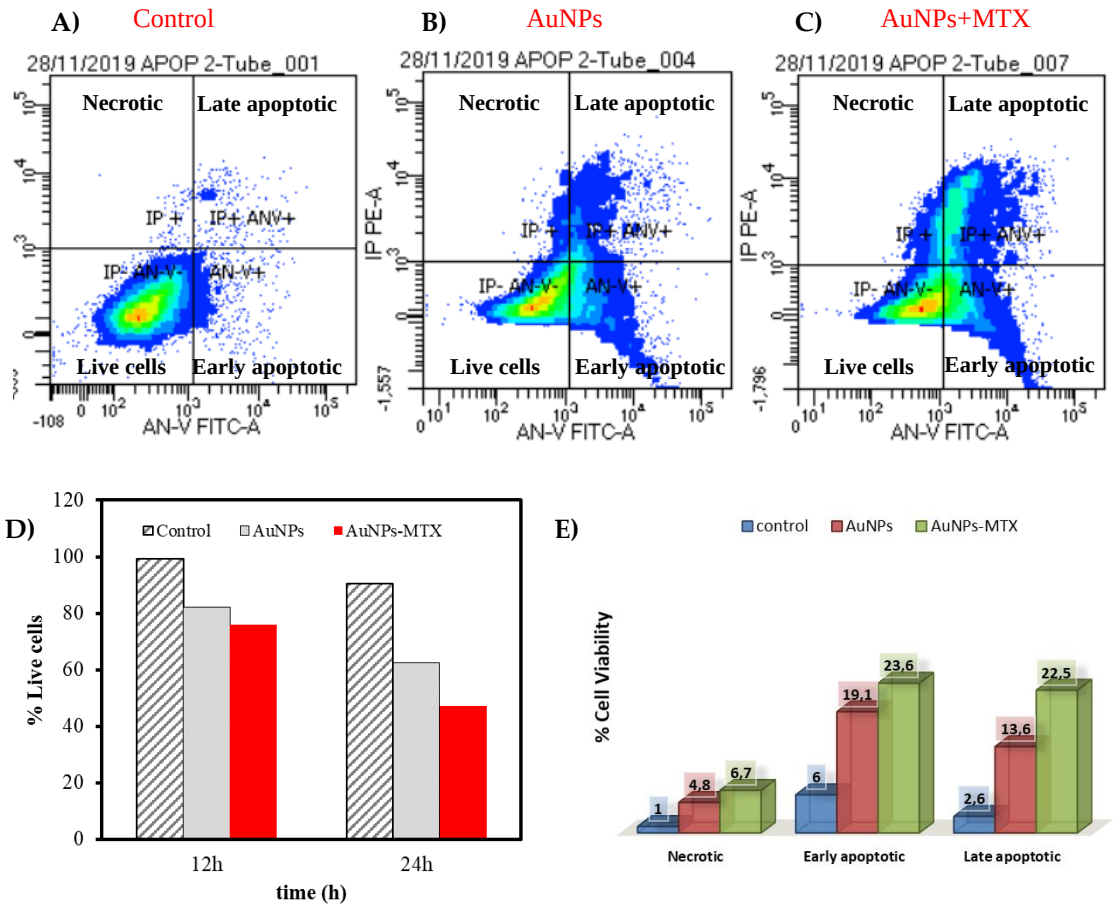

Figure 10. Flow cytometric analysis to determine death modes of cancer cells to HTC-116. The percentage of necrotic and apoptotic HTC-116 cells A) AuNPs and B) AuNPs-MTX400. D) Comparison of time response to equal doses of AuNPs and AuNPs-MTX400. E) Representative percentage of necrotic and apoptotic AuNPs and AuNPs-MTX400.

3. Materials and Methods

3.1. Reagents

Chloroauric acid ($HAuCl_4$), trisodium citrate dehydrate ($Na_3C_6H_5O_7$), methotrexate ($C_{20}H_{22}N_8O_5$) and sodium hydrogen carbonate ($NaHCO_3$) were of analytical grade and used without further purification. All solutions were made using double distilled Milli-Q water (18MΩ).

 doi:10.20944/preprints202011.0440.v1

3.2. Synthesis of gold nanoparticles (AuNPs)

Reference gold nanoparticles have been synthesized based on the methods described in detail elsewhere [12,23]. Briefly 1mL of chloroauric acid dissolution (25 mM) was added to a 150mL of a boiling sodium citrate solution (TCS), (2.2 mM) under vigorous stirring and kept into dark for 12 min at 90 ºC. The mixture color turned fast from pale yellow to light red, indicating the generation of AuNPs. Finally, the resulting colloid was cooled at room temperature, centrifuged at 12000 rpm during 15 min and dried at 60 ºC during 12 hours.

3.3. Synthesis of gold nanoparticles with various MTX contents (AuNPs-MTX)

One step synthesis was undertaken by adding different amounts of a 10 mM MTX solution, made in 1mM K_2CO_3, to the AuNPs solution prepared previously and kept another 10 min at 90 ºC. Finally, the resulting colloid was cooled at room temperature, centrifuged at 12000 rpm during 15 min and dried at 60 ºC during 12 hours. Different concentrations of $AuHCl_4$ and MTX were tested with the aim to determine an optimum ratio (Table 3).

Table 3. Experimental conditions used to synthesize AuNPs and AuNPs-MTX conjugates

				Ratio Au/MTX/TCS			
	$HAuCl_4$	MTX	TCS	$HAuCl_4$	MTX	TCS	pH
		mmol					
AuNPs	0.025	-	0.55	1	-	0.045	8.77
AuNPs-MTX200	0.025	0.0020	0.55	1	0.2	0.045	7.47
AuNPs-MTX300	0.025	0.0030	0.55	1	0.3	0.045	7.65
AuNPs-MTX400	0.025	0.0040	0.55	1	0.4	0.045	7.72

3.4. Characterization of AuNPs and AuNPs-MTX

The reduction of $HAuCl_4$ and the formation of AuNPs were monitored by observing the changes in absorption spectra centered at 520 nm originating from the surface plasmon resonance of the AuNPs using an UV-visible spectroscopy with a VWR UV-1600PC UV/VIS spectrophotometer. Samples were analyzed in the 400–900 nm spectral range. The crystalline structure of AuNPs was examined using a BRUKER D8 ADVANCE diffractometer (Kα Cu) with a LINEXE detector. The chemical structure and functional groups of the AuNPs-MTX were analyzed by Fourier transform infrared spectroscopy (FT-IR, NICOLET 20SXB spectrometer) and recorded in absorbance mode in the 4000–400 cm^{-1} range using a with a spectral resolution of 0.5 cm^{-1}.

X-ray photoelectron spectroscopy (XPS) experiments were conducted on a Kratos Axis Ultra-DLD spectrometer equipped with Al Kα source). CasaXPS software (version 2.3.16) was used to evaluate XPS data.

The size and morphology of AuNPs and AuNPs-MTX were studied with High-resolution transmission electron microscopy (HRTEM) images, obtained using a FEI Titan, operated at 300 kV. SAED patterns were collected using a 10 µm aperture allowing collection of diffraction data from a circular area. Compositional maps of selected areas were acquired in scanning transmission electron microscopy (STEM) mode using a Super X EDX detector (FEI), formed by four windowless SSD detectors. STEM images were collected with a high angle annular dark field (HAADF) detector.

3.5. Short and long term stability test

1 mL of gold colloid solution was mixed with 2 mL of milli Q water, PBS buffer (pH 7.4), Milli-Q water containing 10 % FBS and PBS containing 10 % FBS. After the incubation at 37 ºC for 1, 6, 12

 doi:10.20944/preprints202011.0440.v1

and 24 hours the changes of the maximum absorption wavelength were determined by UV-vis spectroscopy.

Long term storage stability (one month) of prepared silver nanoparticles conjugated with different amounts of methotrexate were also performed after synthesis, keeping samples in the darkness refrigerated at 4 ºC.

3.6. Drug loading capacity

The efficiency of drug conjugation was calculated by a direct method using the absorption of the MTX at 306 nm. Briefly, the unknown drug concentration of the nano-carrier system was determined using a calibration curve based on series of known MTX concentrations. The drug conjugation efficiency was then calculated using following equation [12]:

$$\text{Drug loading } \% = \frac{\text{Initial free MTX added } (g) - \text{MTX measured supernant } (g)}{\text{weight of AgNPs-MTX } (g)} \quad (4)$$

3.7. pH-dependent drug release study

The release profiles for gold nanoparticles conjugated with different amounts of MTX (AuNPs-MTX 200, 300 and 400) were performed by dialysis bags (MWCO 8-14kDa) with phosphate buffer saline (PBS) as release media. 3 mg of Au-MTX conjugates were weighed and introduced in the dialysis bags within 3 mL of PBS and immersed in 80 mL of PBS. The system was shaken at a speed of 150 rpm and incubated at 37 °C. At desired time intervals 3 mL of solution was withdrawn and replaced with and equal volume of fresh buffer. MTX release was then quantified by measuring its absorbance using absorption spectroscopy at 306 nm and the concentration of the drug estimated with the aid of a standard curve. As a control experiment, the release of free MTX from the dialysis bag was also measured.

Finally, the pH effect (pH 7.6 and 5) was studied for the highest concentration conjugated sample (AuNPs-MTX400). Selected conditions simulate physiologic environment (pH 7.4 and 37 °C) and endosomal/lysosomal compartment and cancer tissue environment in vitro (pH 5, 37 °C) [24,25].

3.8. Cytotoxicity and anticancer effect

In vitro bioassays were undertaken with colorectal cancer (HTC-116) (ECACC Nº: 91091005 (lot N° 05K025) and human lung carcinoma (A-549) (ATCC Nº: CCL-185 (lot Nº 3624224) cell lines, obtained from the CIC cell bank of the University of Granada. Cell viability were determined through flow cytometry using a simultaneous double-staining procedure with fluorescein diacetate (FDA) and propidium iodide (PI) in the presence of free MTX, AuNPs and AuNPs-MTX conjugates. 40,000 cells were separately incubated and distributed in 12-well plates for further 24 h incubation at 37 °C in a humid atmosphere enriched with 5% CO_2. The medium was removed, and fresh medium was added together with free MTX (at concentrations of 45.4, 454, 1136 and 4544 μg/mL), AuNPs (887, 1330 and 2260 μg/mL) and AuNPs-MTX (1420, 2130 and 4260 μg/mL). After 12, 24, and 48 hours of treatment 100 μL/well of propidium iodide solution (100 μg/mL) was added and incubated for 10 min at 28 °C in darkness. Afterwards, 100 μL/well of fluorescein diacetate (100 ng/mL) was added and incubated under the same aforementioned conditions. Finally, cells were recovered by centrifugation at 1500 rpm for 10 min and the precipitate was washed with PBS. Flow cytometric analyses were performed with a FACS Vantage™ flow cytometer (Becton Dickinson). The percentage viability was calculated in comparison to the control culture. The IC_{50} values were calculated using linear-regression analysis from the Kc values at the employed concentrations using the software GraphPad Prism 6.

The extent of apoptosis was measured through annexin V-fluorescein isothiocyanate (FITC) apoptosis detection kit as described in the manufacturer's instructions (eBioscience, San Diego, CA). In vitro bioassay was undertaken with colorectal cancer (HTC-116). 10,000 cells were separately incubated and distributed in 12-well plates for further 24 h incubation at 37 °C in a humid atmosphere enriched with 5% CO_2. The medium was removed, and fresh medium was added together with

AuNPs and AuNPs-MTX solutions at different concentrations. After 12, 24, and 48 hours of treatment 5 µL/well of Anexin V was added and incubated for 15 in darkness min in darkness. Afterwards, 5 µL/well of propidium iodide was added and incubated under the same aforementioned conditions. Finally, cells were recovered by centrifugation at 1500 rpm for 10 min and the precipitate was washed with PBS. Flow cytometric analyses were performed with a FACS Vantage™ flow cytometer (Becton Dickinson).

3.9. Statistical analysis

Statistical analysis was performed by using the Graph Pad Prim v.6 software. The one-way analysis of variance (ANOVA) statistical method was used to evaluate the significance of the experimental data. A value of $p < 0.05$ was considered statistically significant.

4. Conclusions

A controlled sized polydisperse AuNPs-MTX conjugate, with an average size of 19.32 ± 4.96 nm and distribution range between 10-31 nm, have been successfully synthesized controlling temperature and pH, and using as reducing agent citrate.

HRTEM mapping showed a homogeneous distribution of Au and N (as an indicator of the MTX presence) with prevalence of a gold nanocrystalline phase (determined by SAED images), which suggests the formation of an Au-MTX conjugate. XPS results confirmed as formation mechanism the chemisorption of MTX through a carboxylic group (-COOH) onto AuNPs via exchange with a citrate molecule.

Calculated drug loading capacity for AuNPs-MTX400 reached 23.6 % releasing 78 % of the initial MTX loaded onto the nanoparticles. MTX conjugated onto AuNPs not only decreased the drug released rate from around 4 hours to 200 hours but also changed from first-order to zero-order kinetic model, allowing a better control of plasma concentration and offering several advantages, including reduction in the frequency of drug administration. Drug release rate also showed a pH stimuli response at acid pHs (5) which could improve penetration into the tumor mass.

Anticancer activity tested in colon and lung cancer cells suggest the effectiveness of drug conjugated AuNPs enhancing the therapeutic effect by inducing apoptosis and decreasing the effective doses in half of MTX in colon cancer cell line, with folate receptor, confirming the MTX mechanism of internalization linking to dihydrofolate reductase (DHFR) and interrupting the folic acid cycle, which is usually overexpressed in cancer cells.

Research manuscripts reporting large datasets that are deposited in a publicly available database should specify where the data have been deposited and provide the relevant accession numbers. If the accession numbers have not yet been obtained at the time of submission, please state that they will be provided during review. They must be provided prior to publication.

Interventionary studies involving animals or humans, and other studies require ethical approval must list the authority that provided approval and the corresponding ethical approval code.

Author Contributions: B.A.G.: Methodology, Formal analysis, Investigation, Software, and Writing-Original Draft; M.F:P.: Methodology, Formal analysis and Software. M.R.: Methodology, Formal analysis, Validation, Software, and Writing-Original Draft; M.F.P.: Methodology and formal analysis. M.S.-P.: Conceptualization, Methodology, Supervision, Project Administration, Resources, Writing-Review, and Editing; M.A.Á.: Formal analysis, Validation, Writing-Review and Software.

Funding: The authors are grateful for the financial support of the Ministry of Science and Innovation and Junta de Andalucia (project P18-RT-4193).

Acknowledgments: The authors thank Dr. Nieves Rodríguez Cabezas and Dr. Jaime Lazuen Alcón (from the CIC-UGR) for helpful advice during cytotoxicity assays design as well as HRTEM and VPSEM technicians Dr. M. del Mar Abad and Dr. Isabel Guerra- Tschuschke (CIC-UGR).

Conflicts of Interest: The authors declare no conflict of interest.

References

1. Han, G.; Ghosh, P.; Rotello, V.M. Functionalized gold nanoparticles for drug delivery. *Nanomed*. **2007**, *2*, 113-123.
2. Ghosh, P.; Han, G.; De, M.; Kim, C.K.; Rotello, V.M. Gold nanoparticles in delivery applications. *Adv. Drug Deliv. Rev.* **2008**, *60*, 1307-1315.
3. Dhar, S.; Liu, Z.; Thomale, J.; Dai, H.; Lippard, S.J. Targeted single-wall carbon nanotube-mediated Pt(IV) prodrug delivery using folate as a homing device. *J. Am. Chem. Soc.* **2008**, *130*, 11467-11476.
4. Kohler, N.; Sun, C.; Fichtenholtz, A.; Gunn, J.; Fang, C.; Zhang, M. Methotrexate-immobilized poly(ethylene glycol) magnetic nanoparticles for MR imaging and drug delivery. *Small* 2006, 2, 785-792.
5. Bleyer, W.A. The clinical pharmacology of methotrexate: new applications of an old drug. *Cancer* **1978**, 41, 36-51.
6. Young, K.L.; Xu, C.; Xie, J.; Sun, S. Conjugating methotrexate to magnetite (Fe(3)O(4)) nanoparticles via trichloro-s-triazine. *J. Mater. Chem.* **2009**, *19*, 6400-6406.
7. Bessar, H.; Venditti, I.; Benassi, L.; Vaschieri, C.; Azzoni, P.; Pellacani, G.; Magnoni, C.; Botti, E.; Casagrande, V.; Federici, M.; Costanzo, A.; Fontana, L.; Testa, G.; Mostafa, F.F.; Ibrahim, S.A.; Russo, M.V.; Fratoddi, I. Functionalized gold nanoparticles for topical delivery of methotrexate for the possible treatment of psoriasis. *Colloids Surf. B Biointerfaces* **2016**, *141*, 141-147.
8. Chen, Y.-H.; Tsai, C.-Y.; Huang, P.-Y.; Chang, M.-Y.; Cheng, P.-C.; Chou, C.-H.; Chen, D.-H.; Wang, C.-R.; Shiau, A.-L.; Wu, C.-L. Methotrexate conjugated to gold nanoparticles inhibits tumor growth in a syngeneic lung tumor model. *Mol. Pharm.* **2007**, *4*, 713-722.
9. Dey, S.; Sherly, M.C.D.; Rekha, M.R.; Sreenivasan, K. Alginate stabilized gold nanoparticle as multidrug carrier: Evaluation of cellular interactions and hemolytic potential. *Carbohydr. Polym.* **2016**, *136*, 71-80.
10. Murawala, P.; Tirmale, A.; Shiras, A.; Prasad, B.L.V. In situ synthesized BSA capped gold nanoparticles: Effective carrier of anticancer drug methotrexate to MCF-7 breast cancer cells. *Mater. Sci. Eng. C* **2014**, *34*, 158-167.
11. Tran, N.T.T.; Wang, T.-H.; Lin, C.-Y.; Tai, Y. Synthesis of methotrexate-conjugated gold nanoparticles with enhanced cancer therapeutic effect. *Biochem. Eng. J.* **2013**, *78*, 175–180.
12. Wang, W.-Y.; Zhao, X.-F.; Ju, X.-H.; Wang, Y.; Wang, L.; Li, S.-P.; Li, X.-D. Novel morphology change of Au-Methotrexate conjugates: From nanochains to discrete nanoparticles. *Int. J. Pharm.* **2016**, *515*, 221-232.
13. Akhter, S.; Ahmad, M.Z.; Ahmad, F.J.; Storm, G.; Kok, R.J. Gold nanoparticles in theragnostic oncology: current state-of-the-art. *Expert Opin. Drug Deliv.* **2012**, *9*, 1225–1243.
14. Arvizo, R.; Bhattacharya, R.; Mukherjee, P. Gold nanoparticles: Opportunities and challenges in nanomedicine. *Expert Opin. Drug Deliv.* **2010**, *7*, 753-763.
15. Boisselier, E.; Astruc, D. Gold nanoparticles in nanomedicine: preparations, imaging, diagnostics, therapies and toxicity. *Chem. Soc. Rev.* **2009**, *38*, 1759-1782.
16. Huang, X.; Jain, P.K.; El-Sayed, I.H.; El-Sayed, M.A. Gold nanoparticles: interesting optical properties and recent applications in cancer diagnostics and therapy. *Nanomed*. **2007**, *2*, 681-693.
17. Rana, S.; Bajaj, A.; Mout, R.; Rotello, V.M. Monolayer coated gold nanoparticles for delivery applications. *Adv. Drug Deliv. Rev.* **2012**, *64*, 200-216.
18. Podsiadlo, P.; Sinani, V.A.; Bahng, J.H.; Kam, N.W.S.; Lee, J.; Kotov, N.A. Gold nanoparticles enhance the anti-leukemia action of a 6-mercaptopurine chemotherapeutic agent. *Langmuir* **2008**, *24*, 568-574.
19. Ulbrich, K.; Etrych, T.; Chytil, P.; Pechar, M.; Jelinkova, M.; Rihova, B. Polymeric anticancer drugs with pH-controlled activation. *Int. J. Pharm.* **2004**, *277*, 63-72.
20. Hong, R.; Han, G.; Fernández, J.M.; Kim, B.; Forbes, N.S.; Rotello, V.M. Glutathione-mediated delivery and release using monolayer protected nanoparticle carriers. *J. Am. Chem. Soc.* **2006**, *128*, 1078-1079.
21. Hostetler, M.J.; Templeton, A.C.; Murray, R.W. Dynamics of place-exchange reactions on monolayer-protected gold cluster molecules. *Langmuir* **1999**, *15*, 3782-3789.
22. Moaseri, E.; Bollinger, J.A.; Changalvaie, B.; Johnson, L.; Schroer, J.; Johnston, K.P.; Truskett, T.M. Reversible self-assembly of glutathione-coated gold nanoparticle clusters via pH-tunable interactions. *Langmuir* **2017**, *33*, 12244-12253.
23. Bastús, N.G.; Comenge, J.; Puntes, V. Kinetically controlled seeded growth synthesis of citrate-stabilized gold nanoparticles of up to 200 nm: Size focusing versus Ostwald ripening. *Langmuir* **2011**, *27*, 11098-11105.

24. Cheng, R.; Meng, F.; Deng, C.; Klok, H.-A.; Zhong, Z. Dual and multi-stimuli responsive polymeric nanoparticles for programmed site-specific drug delivery. *Biomaterials* **2013**, *34*, 3647-3657.
25. Yang, Y.; Lin, Y.; Di, D.; Zhang, X.; Wang, D.; Zhao, Q.; Wang, S. Gold nanoparticle-gated mesoporous silica as redox-triggered drug delivery for chemo-photothermal synergistic therapy. *J. Colloid Interface Sci.* **2017**, *508*, 323-331.
26. Sharma, J.; Tai, Y.; Imae, T. Biomodulation approach for gold nanoparticles: Synthesis of anisotropic to luminescent particles. *Chem. Asian J.* **2010**, *5*, 70-73.
27. Shen, J.-J.; Zhang, P.-H.; Zheng, F.; Chen, H.; Chen, W.; Ding, Y.; Xia, X.-H. Preliminary quality criteria of citrate-protected gold nanoparticles for medicinal applications. *ACS Appl. Nano Mater.* **2018**, *1*, 2120-2128.
28. Liang, M.; Lin, I.-C.; Whittaker, M.R.; Minchin, R.F.; Monteiro, M.J.; Toth, I. Cellular uptake of densely packed polymer coatings on gold nanoparticles. *ACS Nano* **2010**, *4*, 403-413.
29. Ayyappan, S.; Sundaraganesan, N.; Aroulmoji, V.; Murano, E.; Sebastian, S. Molecular structure, vibrational spectra and DFT molecular orbital calculations (TD-DFT and NMR) of the antiproliferative drug Methotrexate. *Spectrochim. Acta. A. Mol. Biomol. Spectrosc.* **2010**, *77*, 264-275.
30. Chandni, K; Andhariya, N.; Pandey, O.P.; Chudasama, B. A growth kinetic study of ultrafine monodispersed silver nanoparticles. *RSC Adv.* **2012**, *3*, 1127-1136.
31. Alexander, M.R.; Payan, S.; Duc, T.M. Interfacial interactions of plasma-polymerized acrylic acid and an oxidized aluminium surface investigated using XPS, FTIR and poly(acrylic acid) as a model compound. *Surf. Interface Anal.* **1998**, *26*, 961-973.
32. Frydman, E.; Cohen, H.; Maoz, R.; Sagiv, J. Monolayer damage in XPS measurements as evaluated by independent methods. *Langmuir* **1997**, *13*, 5089-5106.
33. Nosrati, H.; Salehiabar, M.; Davaran, S.; Danafar, H.; Manjili, H.K. Methotrexate-conjugated L-lysine coated iron oxide magnetic nanoparticles for inhibition of MCF-7 breast cancer cells. *Drug Dev. Ind. Pharm.* **2018**, *44*, 886-894.
34. Asokan, A.; Cho, M.J. Exploitation of intracellular pH gradients in the cellular delivery of macromolecules. *J. Pharm. Sci.* **2002**, *91*, 903-913.
35. Gerweck, L.E.; Vijayappa, S.; Kozin, S. Tumor pH controls the in vivo efficacy of weak acid and base chemotherapeutics. *Mol. Cancer Ther.* **2006**, *5*, 1275-1279.
36. Dominska, M.; Dykxhoorn, D.M. Breaking down the barriers: siRNA delivery and endosome escape. *J. Cell Sci.* **2010**, *123*, 1183-1189.
37. Whitehead, K.A.; Langer, R.; Anderson, D.G. Knocking down barriers: advances in siRNA delivery. *Nat. Rev. Drug Discov.* **2009**, *8*, 129-138.
38. Gokhale, A. Achieving zero-order release kinetics using multi-step diffusion-based drug delivery. *Pharm. Tech.* **2014**, *26*, 38-42.
39. Brown, J.M.; Attardi, L.D. The role of apoptosis in cancer development and treatment response. *Nat. Rev. Cancer* **2005**, *5*, 231-237.